NJC

ROYAL SOCIETY OF CHEMISTRY

PAPER

View Article Online
View Journal | View Issue

Cite this: *New J. Chem.*, 2024, **48**, 2743

Structural and thermodynamic investigations of $Zr(BH_4)_4$ and $Hf(BH_4)_4$ between 280 K and their decomposition temperatures†

Konrad Burkmann,[a] Franziska Habermann,[a] Erik Schumann,[a] Jakob Kraus,[b] Bianca Störr,[a] Horst Schmidt,[cd] Erica Brendler,[e] Jürgen Seidel,[a] Klaus Bohmhammel,[a] Jens Kortus[b] and Florian Mertens*[af]

Received 5th December 2023,
Accepted 8th January 2024

DOI: 10.1039/d3nj05601e

rsc.li/njc

The borohydrides of zirconium ($Zr(BH_4)_4$) and hafnium ($Hf(BH_4)_4$) have been prepared by solid state metatheses. The crystal structures were determined slightly below their melting temperature with *in situ* cryo crystallisation single crystal XRD. The melting and decomposition process was investigated using differential scanning calorimetry coupled with thermogravimetry and mass spectroscopy. The enthalpies of formation were determined using the decomposition enthalpy, the enthalpy of fusion and the heat capacity measurements in the temperature range from 5 °C to 35 °C. Standard entropy values of both compounds were obtained by DFT calculations. The determined values were optimised using the CalPhaD method.

Introduction

Complex hydrides are still in the focus of current research in the field of hydrogen storage.[1,2] The covalent borohydrides $Zr(BH_4)_4$ and $Hf(BH_4)_4$ possess melting points of about 30 °C[3] and therefore have been considered as volatile precursors to produce thin layers of ZrB_2 and HfB_2 *via* chemical vapor deposition for a long time.[4–9] Consequently, a significant number of reports on the decomposition of these borohydrides under relatively harsh conditions (high temperatures from the gas phase) have been published so far. To our knowledge, however, there is only one investigation of the decomposition behaviour of $Zr(BH_4)_4$ under atmospheric conditions reported by Gennari *et al.*[10] and none in regard to $Hf(BH_4)_4$. Furthermore, neither experimental data in respect to the enthalpy of formation nor the absolute entropy of the two compounds nor to their heat capacity functions can be found. However, the melting and extrapolated boiling points as well as the heat of fusion, vaporisation and sublimation were determined by Hoekstra and Katz.[3]

Besides the application as CVD precursors, these borohydrides are currently also used to functionalise surfaces to generate polymerisation and hydrogenation catalysts.[11] In respect to the development of metal hydride systems for hydrogen storage, *i.e.* to generate systems that allow the uptake and release of hydrogen by acceptable pressure and/or temperature variation, it is important to extend the database of thermodynamic values of complex metal hydrides. A way to arrive at such systems is by creating reactive hydride mixtures (often called reactive hybrids) to implement the concept of thermodynamic tuning.[12–15] This concept is based on the idea to achieve reversibility of the hydrogenation by the enthalpic contribution of the reaction of the dehydrogenated hydrides. The option to use Zr and Hf as catalysts for the (re)hydrogenation reactions of complex metal hydrides by adding them as halides,[16] adds to the importance of understanding and exploring the decomposition behaviour and the thermodynamics of their complex metal hydrides such as their boranates and alanates.

The synthesis procedures mentioned in the following can be used for the generation of $Zr(BH_4)_4$ and $Hf(BH_4)_4$. Numerous authors report various liquid phase syntheses of $Zr(BH_4)_4$ and $Hf(BH_4)_4$. Wayda *et al.*,[5] James and Smith,[17] Sayer *et al.*[18] and Smith *et al.*[19] used $ZrCl_4$ and $LiBH_4$ in diethyl ether according to reaction (1) (M = Zr). It was then possible to use fractional

[a] *Institut für Physikalische Chemie, TU Bergakademie Freiberg, Leipziger Straße 29, 09599 Freiberg, Germany. E-mail: florian.mertens@chemie.tu-freiberg.de; Tel: +493731-393737*
[b] *Institut für Theoretische Physik, TU Bergakademie Freiberg, Leipziger Straße 23, 09599 Freiberg, Germany*
[c] *Institut für Anorganische Chemie, TU Bergakademie Freiberg, Leipziger Straße 29, 09599 Freiberg, Germany*
[d] *Institut für Technische Chemie, TU Bergakademie Freiberg, Leipziger Straße 29, 09599 Freiberg, Germany*
[e] *Institut für Analytische Chemie, TU Bergakademie Freiberg, Leipziger Straße 29, 09599 Freiberg, Germany*
[f] *Zentrum für effiziente Hochtemperatur-Stoffwandlung, TU Bergakademie Freiberg, Winklerstraße 5, 09599 Freiberg, Germany*

† Electronic supplementary information (ESI) available. CCDC 2173083 and 2173084. For ESI and crystallographic data in CIF or other electronic format see DOI: https://doi.org/10.1039/d3nj05601e

distillation for the purification of both compounds because of their low melting points and their high vapour pressures.[3] Wayda *et al.*[5] and Broach *et al.*[20] used the same method for the preparation of $Hf(BH_4)_4$ (M = Hf). Hoekstra and Katz[3] further report reactions of $ZrCl_4$ (or $HfCl_4$, respectively) with $Al(BH_4)_3$ (see reaction (2), M = Zr, Hf) or with $NaZrF_5$ (see reaction (3), M = Zr, Hf). The last method mentioned was also applied by Reid *et al.* using $KZrF_5$.[21] Banks *et al.* used Na_2ZrF_6 and $Al(BH_4)_3$ to produce $Zr(BH_4)_4$ in the same manner.[22]

$$4\ LiBH_4 + MCl_4 \rightarrow M(BH_4)_4 + 4\ LiCl \quad (1)$$

$$4\ Al(BH_4)_3 + 3\ MCl_4 \rightarrow 3\ M(BH_4)_4 + 4\ AlCl_3 \quad (2)$$

$$2\ Al(BH_4)_3 + NaMF_5 \rightarrow M(BH_4)_4 + 2\ AlF_2BH_4 + NaF \quad (3)$$

Banks *et al.* mentioned problems with the purification and metathesis reaction (2), which occurred incomplete and with reaction (3) taking several days to finish.[22] Reid *et al.* reported the synthesis from $Zr(OR)_4$ with gaseous B_2H_6 (see reaction (4)).[21]

$$3\ Zr(OR)_4 + 8\ B_2H_6 \rightarrow 3\ Zr(BH_4)_4 + 4\ B(OR)_3 \quad (4)$$

$Zr(BH_4)_4$ can also be prepared by mixing $ZrCl_4$ with $LiBH_4$ in a flask and heating the mixture above the melting point of $Zr(BH_4)_4$ at 29 °C, according to Rice and Woodin (see reaction (1)).[4] The synthesis of $Hf(BH_4)_4$ can be conducted analogously. Several authors used this method, too.[6,21–30] All mentioned groups separated the product ($Zr(BH_4)_4$) from the by-product (LiCl) by sublimation into a cold trap exploiting the high vapour pressure of the solid phase at room temperature of about 20 mbar.[3] Various authors employed ball milling of $LiBH_4$ (or $NaBH_4$) with $ZrCl_4$ to produce mixtures of $Zr(BH_4)_4$, $LiBH_4$ (or $NaBH_4$) and LiCl (or NaCl).[10,31–33] Some of them used sublimation for separation and purification of the $Zr(BH_4)_4$.[10,31] Volkov *et al.* applied vacuum rotation milling to prepare these compounds.[34]

We applied the direct metathesis route according to reaction (1) to prepare $Zr(BH_4)_4$ and $Hf(BH_4)_4$ because of the simplicity of the implementation and purification of the target compounds using this method. We investigated the melting and decomposition behaviour of both compounds including the resulting decomposition products using thermoanalysis, evolved gas analysis, X-ray diffraction and SEM-EDX. Furthermore, heat capacity measurements were performed and density functional theory was chosen to calculate entropy values resulting in a large set of thermodynamic data for both compounds. Additionally, we report the crystal structures of both compounds measured slightly below their melting temperature.

Experimental section

Materials and methods

All handling and manipulation of the chemicals as well as the sample preparation for the measurements were performed in an argon (Nippon Gases, 5N) filled glove box with a gas circulation purifying system (H_2O and O_2 < 0.1 ppm) from MBraun or at an argon filled Schlenk line.[35,36]

Lithiumborohydride ($LiBH_4$, Chemetall), zirconium tetrachloride ($ZrCl_4$, Merck, anhydrous for synthesis) and hafnium tetrachloride ($HfCl_4$, Alfa Aesar, 98+%, metals basis excluding Zr, Zr < 2.7%) were used as received. Deuterated benzene (C_6D_6, DEUTERO, 99%) and benzene (C_6H_6, CARL ROTH, ≥ 99.5%) were distilled from Na/Al_2O_3 (SOLVONA, Dr Bilger Umweltconsulting, Germany) and benzophenone ($C_{13}H_{10}O$, SIGMA-ALDRICH, 99%). Tetrahydrofurane (C_4H_8O, VWR International GmbH, 99%) and deuterated tetrahydrofurane (C_4H_8O, DEUTERO, 99.5%) were dried over a 4 Å molecular sieve. Zirconocen dibromide (Cp_2ZrBr_2) was used as reference material for the ^{91}Zr NMR investigations. Sapphire (aluminium oxide, Al_2O_3) was used as reference material for the heat capacity measurements.

Characterisation techniques

Nuclear magnetic resonance (NMR) spectroscopy. ^1H (500.13 MHz), ^{11}B (160.46 MHz) and ^{91}Zr (46.49 MHz) NMR spectra were acquired with a Bruker Avance III 500 MHz spectrometer. The chemical shifts (in ppm) for ^1H spectra are given relative to $SiMe_4$, for ^{11}B relative to 15 Vol–% $BF_3{\cdot}Et_2O$ in $CDCl_3$ and for ^{91}Zr relative to Cp_2ZrBr_2 in a 1:4 THF-d_8:THF mixture (0.2 mol L^{-1}; = 0 ppm) as used by Böhme *et al.*,[37] whereby all references were used as an external standard. NMR data were measured in Young tubes due to the air and moisture sensitivity of the samples and processed by using Bruker TopSpin 4.0.7. The samples were dissolved in C_6D_6 (for ^1H and ^{11}B) or 1:4 C_6D_6:C_6H_6 mixtures (for ^{91}Zr).

Single crystal *in situ* cryo crystallisation X-ray diffraction (SC-XRD). We used glass capillaries (''Markröhrchen'') with 0.5 mm diameter from Hilgenberg for the single crystal structure determination. Data collections were performed on a STOE IPDS-II image plate diffractometer equipped with a low-temperature device using Mo-K_α radiation (λ = 0.71073 Å) with ω and ϕ scans. The method described by Gerwig *et al.* was applied to prepare the samples and to get single crystals *via in situ* cryo crystallisation in the capillary.[38]

Powder X-ray diffraction (P-XRD). The measurements were performed on a D2 Phaser diffractometer from Bruker (15° to 85° 2θ, 0.05° 2θ steps, dwell time 1 s, 300 W X-ray power) equipped with a LYNXEYE detector with Cu-K_α radiation (λ = 1.54184 Å). The powders were ground with a mortar and pestle and placed on a single crystal silicon sample holder.

Scanning electron microscopy-energy dispersive X-ray spectroscopy (SEM-EDX). Prior to the measurements all samples were coated with carbon to ensure a good electrical conductivity of the sample and a good electrical contact between the sample and the sample holder. The SEM-EDX measurements were performed in high vacuum using a JSM-7001F electron microscope from JOEL with 3 kV acceleration voltage. For mapping and surface quantification a Quantax EDX detector from BRUKER NANO GmbH was used with an acceleration voltage of 15 kV.

Simultaneous thermogravimetry-differential scanning calorimetry coupled with mass spectroscopy (TG-DSC-MS). The TG-DSC-MS measurements (about 10 mg of sample;

corundum crucibles; heating/cooling rate of 5 K min^{-1}; argon purge gas flow of 20 mL min^{-1}) were performed on a Sensys TGA-DSC from SETARAM, France coupled with a Pfeiffer Omnistar Quadrupol mass spectrometer (MS). The MS was used to determine the gaseous decomposition products such as hydrogen and diborane. The data processing was carried out with the Calisto v1.065 instrument software.

Thermal analysis and calorimetric heat capacity measurement. All thermal investigations were performed in a DSC 111 from SETARAM, France using the instrument software (Calisto, AKTS/SETARAM) to conduct the data evaluation. The thermal analysis was carried out in sealed stainless steel high pressure crucibles in the temperature range from 8 °C to 325 °C with about 35 mg to 50 mg of sample material. Since the apparent onset temperature depends on the heating rate, the melting temperatures used in the evaluations further down were obtained by extrapolating the onset temperatures back to a heating rate of 0 K min^{-1}.

Measurements of the heat capacity of the solids and melts were performed inspired by the method already described by various authors.[39–45] In detail, about 120 mg of the sample were filled into standard stainless steel sample vessels. Using a nickel sealing the vessels were crimped tightly. The nickel sealings and the vessels were brought to an identical mass by hand polishing to avoid variations in the blank effects. A C_P-by-step method based on six temperature steps (3.75 K, 3 K min^{-1}) in the temperature range from 6 °C to 36 °C each followed by an isothermal period of 60 min duration was carried out. This temperature programme was applied to the measurements of the sample, the reference (sapphire) and the blank, which was an empty steel vessel. Using the recommended reference heat capacity of sapphire from ref. 46 the heat capacities of both samples were calculated *via* eqn (5),

$$\overline{C}_{p,i} = \frac{\int_{t_i}^{t_{i+1}} \dot{Q}_{sample}\mathrm{d}t - \int_{t_i}^{t_{i+1}} \dot{Q}_{blank}\mathrm{d}t}{\int_{t_i}^{t_{i+1}} \dot{Q}_{ref}\mathrm{d}t - \int_{t_i}^{t_{i+1}} \dot{Q}_{blank}\mathrm{d}t} \cdot \frac{m_{ref}}{m_{sample}} \cdot \overline{C}_{p,ref,i} \qquad (5)$$

whereby $\bar{C}_p$ defines the specific heat capacity of the sample at the mean temperature of the ramp. The start and end time of the heat flow $\dot{Q}$ peaks are denoted by t_i and t_{i+1}. The masses of the sample and reference material are labeled m_{sample} and m_{ref}, respectively. Finally, $\bar{C}_{p,ref}$ is used as the specific heat capacity of the reference material at the mean temperature of the ramp. Each compound was measured four times.

Synthesis procedures

Lithium borohydride and the corresponding transition metal tetrachloride (zirconium tetrachloride or hafnium tetrachloride) were mixed in stoichiometric amounts under protective atmosphere (see reaction (1)) in a Schlenk vessel. The vessel was transferred to a Schlenk line and the two solids were stirred for 2 h to 4 h at about 50 °C to 70 °C (oil bath). After that measure, the product was distilled in vacuum into a cold trap and stored in a glove box (about 60% yield). After a few days large crystals grew on the wall of the storage vials. These crystals were used for the previously mentioned measurements.

Density functional theory (DFT) calculations

All density functional theory calculations (DFT[47,48]) were performed using the Quantum ESPRESSO code,[49–51] version 6.7. In these calculations, PAW pseudopotentials[52] were employed, which were taken from the PSlibrary,[53] version 1.0.0. The PAW pseudopotentials were combined with the PBE[54] generalized-gradient exchange–correlation functional.

Results and discussion

NMR measurements

The success of the syntheses and the purity of both compounds were verified using NMR spectroscopy. For comparison of the measured chemical shifts with already known values from the literature, those regarding ^{1}H and ^{11}B NMR are listed in Table 1. If necessary, the literature values were adapted to reference compounds we used.

The reported chemical shifts of the signals in the ^{1}H NMR spectra exhibit only small differences in respect to our data (see Table 1), which is possible due to differences in solvent and concentration. Besides, the chemical shifts for the ^{11}B nuclei determined by us fit well with the data from literature for both transition metal borohydrides.

For ^{91}Zr we obtained a chemical shift of δ = 44.1 ppm, which is in good agreement with the already published literature value of 40.7 ppm.[18] For the Hf nuclei, there are no NMR data available. The two NMR active nuclei of Hf (^{177}Hf and ^{179}Hf) exhibit large quadrupole moments,[58] resulting in strong line broadenings. For this reason, no Hf NMR data are presented in this paper.

All measured spectra can be found in the ESI† Fig. S1 to S3. The already known coupling patterns are observable in the ^{1}H (Fig. S1, ESI†) and ^{11}B (Fig. S2, ESI†) NMR spectra. From our measurements, it can be concluded that both compounds were synthesised with sufficient purity.

Structure determination sligthly below the melting temperature and calculation of the cubic thermal expansion coefficient

Both boranates have already been crystallographically characterised, $Zr(BH_4)_4$ at 100 K[31] and $Hf(BH_4)_4$ at 110 K,[20] and crystallise in the cubic space group $P\bar{4}3m$. In order to exclude a possible phase transition in the temperature range up to a temperature close to the starting point of our DSC measurements, both boranates were subjected to an SC-XRD

Table 1 Comparison of measured values for the ^{1}H and ^{11}B chemical shifts δ with literature values

Compound	$\delta(^1H)$ [ppm]	$\delta(^{11}B)$ [ppm]	Method	Ref.
$Zr(BH_4)_4$	1.61		Experimental	23
		−8.0	Experimental	18
		−8.5	Experimental	55 and 56
		−8.0	DFT	57
	1.50	−8.2	Experimental	This work
$Hf(BH_4)_4$	2.88	−11.0	Experimental	23
		−11.0	Experimental	55
		−14.7	Experimental	55 and 56
	2.70	−11.3	Experimental	This work

investigation. Table 2 shows the results of the measurements and the structures are additionally displayed in Fig. S4 (ESI†).

From the listed data in this table, a fundamental change of the crystal structure besides the thermal expansion can be excluded. A molecular dynamic simulation by Igoshkin *et al.* supports this result.[60] As can be expected, the displacement parameters are enlarged at these high temperatures, especially for $Zr(BH_4)_4$, which can be explained by the proximity to the melting point. For more structure related details the reader is referred to the literature.[20,31]

Additionally, the cubic thermal expansion coefficient γ has been calculated (eqn (7)[61]) from the data given in the literature[20,31] and our own results.

$$\gamma = \frac{1}{V} \cdot \left(\frac{\partial V}{\partial T}\right)_P \quad (6)$$

$$\gamma = \frac{1}{V_0} \frac{\Delta V}{\Delta T} \quad (7)$$

The molar volumes V were calculated using the molar mass and the density (derived from the SC-XRD measurement). We calculated a cubic thermal expansion coefficient of $\gamma = 37.0 \cdot 10^{-5}$ K^{-1} and of $\gamma = 27.2 \cdot 10^{-5}$ K^{-1} for $Zr(BH_4)_4$ at 273 K and for $Hf(BH_4)_4$ at 288 K, respectively. These values deviate strongly from those of typical inorganic ionic compounds which can be seen as an indicator, besides the low melting point, for the molecular nature of the compounds.[62]

Thermal investigation of the melting and decomposition events using DSC measurements

$Zr(BH_4)_4$. The melting of the sample was investigated with DSC measurements. Heating the material at a rate of 1 K min^{-1}, a sharp signal with the onset point at 28.10 °C indicating the melting of the material (see Fig. 1, lower part) is observed. The melting enthalpy was determined to be 13.25 kJ mol^{-1}. This value differs from the melting enthalpy value of 18 kJ mol^{-1} reported by Hoekstra and Katz[3] which was derived from the difference between the sublimation and vaporisation enthalpies obtained from vapour pressure measurements with only a few measured data points. Unfortunately, no more data on melting enthalpies have been published. The cooling curves exhibit the solidification peak onset temperature at lower values than the melting onset temperature which is typical for solidification processes (supercooling).

Another measurement with new material at a different heating rate of 5 K min^{-1} between 8 °C and 325 °C was used for the extrapolation of the heating rate to 0 K min^{-1} resulting in a melting temperature of 27.94 °C. Furthermore, the decomposition temperature and the released heat during decomposition after the melting was measured. It is noteworthy to mention that the released heat cannot be equated with the decomposition enthalpy since there may have been a pressure built up in the closed crucibles. The value of $\Delta_{dec}U$ = 56.94 kJ mol^{-1} can be taken from Fig. 1. We decided to use a heating rate of 5 K min^{-1} instead of 1 K min^{-1} to prevent very broad signals as mentioned by Gennari *et al.*[10] The decomposition does not appear to be reversible since there are no exothermic effects visible during the cooling phase indicating hydrogen uptake. Table 3 serves as a summary of all so far reported melting and decomposition temperatures.

The melting temperature determined by the extrapolation method described above fits well to the corresponding values in the literature. In contrast, the obtained decomposition

Table 2 Crystallographic and structure refinement data for $Zr(BH_4)_4$ and $Hf(BH_4)_4$

	Zirconium(IV) borohydride	Hafnium(IV) borohydride
Empirical formula	$Zr(BH_4)_4$	$Hf(BH_4)_4$
Formular weight	150.595	237.861
Crystal system,	Cubic,	Cubic,
Space group	$P\bar{4}3m$	$P\bar{4}3m$
Temperature (K)	273	288
a (Å)	5.955 ± 0.011	5.9464 ± 0.0010
V (Å^3)	211.1 ± 1.2	210.27 ± 0.62
Z	1	1
Radiation type	Mo-K_α	Mo-K_α
μ (mm^{-1})	1.19	12.45
Data collection		
Diffractometer	STOE IPDS 2	STOE IPDS 2
Absorption correction	—	Integration[59]
No. of measured,	3767	2072
Independent and observed	115	135
$[I > 2\sigma(I)]$ reflections	115	135
R_{int}	0.133	0.081
$(\sin\theta/\lambda)_{max}$ (Å^{-1})	0.645	0.696
Refinement		
$R[F2 > 2\sigma(F2)]$, $wR(F2)$, S	0.011, 0.027, 1.05	0.034, 0.095, 1.05
No. of reflections	115	135
No. of parameters	12	12
No. of restraints		2
H-atom treatment	All H-atom parameters refined	All H-atom parameters refined
$\Delta\rho_{max}$, $\Delta\rho_{min}$ (e Å^{-3})	0.09, −0.07	0.91, −0.78
Absolute structure	Refined as an inversion twin.	Refined as an inversion twin.

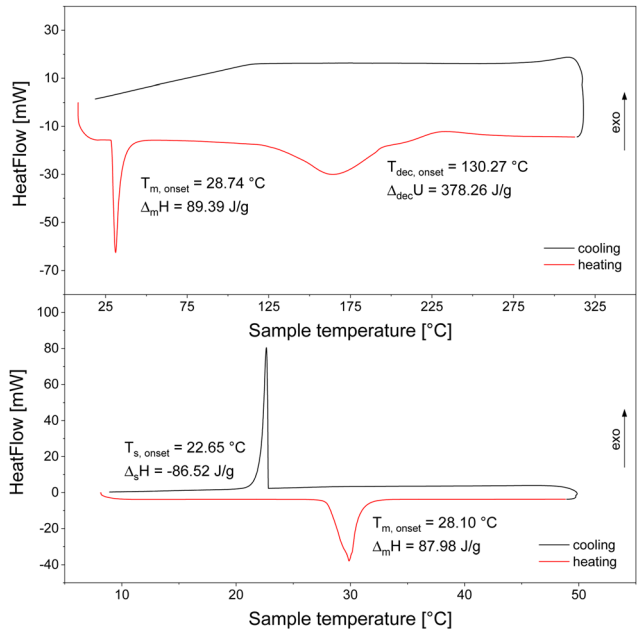

Fig. 1 DSC measurements to investigate the melting (bottom; heating/cooling rate of 1 K min^{-1} from 8 °C to 50 °C; 41.79 mg sample) and decomposition behaviour (top; heating/cooling rate of 5 K min^{-1} from 8 °C to 325 °C; 28.67 mg sample) of $Zr(BH_4)_4$ in closed crucibles.

temperature is about 40 K higher than the one given by Gennari *et al.*[10] and even 50 K higher than that by Nakamori *et al.*[32] An explanation for these discrepancies could be the use of a sealed instead of an open crucible as was used by Gennari *et al.*[10] Utilising open crucibles leads in the investigated systems to a remarkable loss of sample due to evaporation of the molten material before its decomposition. We prevented this problem by using sealed crucibles. The disadvantage, however, of this mode of operation is the shift of the decomposition temperature to higher values due to the rise of the pressure in the gas phase caused by the evaporated material. The decomposition event occurs at an onset temperature of 130.27 °C with broad signals, because it is a decomposition from the liquid state and it is not clear if the decomposition happens as a multi-step process. Further discussion and evaluation of the decomposition is presented in the next section.

$Hf(BH_4)_4$

To our knowledge, there are no DSC measurements of $Hf(BH_4)_4$ available in the literature. Fig. 2 displays a heating and cooling cycle in the lower part, which exhibits a sharp melting point at 28.57 °C (heating rate of 1 K min^{-1}) with a melting enthalpy of 13.49 kJ mol^{-1}. This value is in good agreement with the value from Hoekstra and Katz of 14.24 kJ mol^{-1}[3] obtained from vapour pressure measurements. The cooling curve exhibits the solidification peak at somewhat lower temperatures than the liquidification peak which is typical for solidification processes because of supercooling. After having extrapolated the heating rate to 0 K min^{-1} applying the same procedure as mentioned above we determined the melting temperature to be 28.43 °C.

The melting temperature determined also agrees well to what was published by other groups.[3,56] Regarding the decomposition temperature, however, there are values obtained from chemical vapour deposition experiments reported (also listed in Table 4) that strongly deviate from each other, but no value from a direct thermal analysis is available. Since the values obtained by CVD are inconsistent and the exact knowledge of the decomposition temperature and decomposition enthalpy are a prerequisite for the investigation of the whole decomposition process, we determined precisely the decomposition temperature as well as the decomposition heat similarly as it was done for $Zr(BH_4)_4$ in another measurement (see upper part of Fig. 2) from our DSC measurement. Analogously to $Zr(BH_4)_4$, the irreversible decomposition occurred in the liquid phase resulting in a very broad signal ($T_{dec,onset}$ = 136.44 °C and $\Delta_{dec}U$ = 76.24 kJ mol^{-1}). Looking at the shape of the signal, it seems that the decomposition occurs in a multi-step process, presumable just in a two-step one. Further discussion and evaluation is presented in the next section.

Table 3 Summary of the measured temperatures both for melting T_m and decomposition T_{dec} of $Zr(BH_4)_4$ with literature values (CVD: chemical vapour deposition)

T_m [°C]	Method	T_{dec} [°C]	Method	Ref.
28.7	Vapor pressure	—	—	3
28.7	Not mentioned	—	—	21
28.5	Not mentioned	—	—	56
31.85	DSC, capillary	81.85	DSC	10
—	—	100	CVD	5
—	—	195	TDS	32
—	—	126.85	MDS	60
27.94	DSC	130.27	DSC	This work

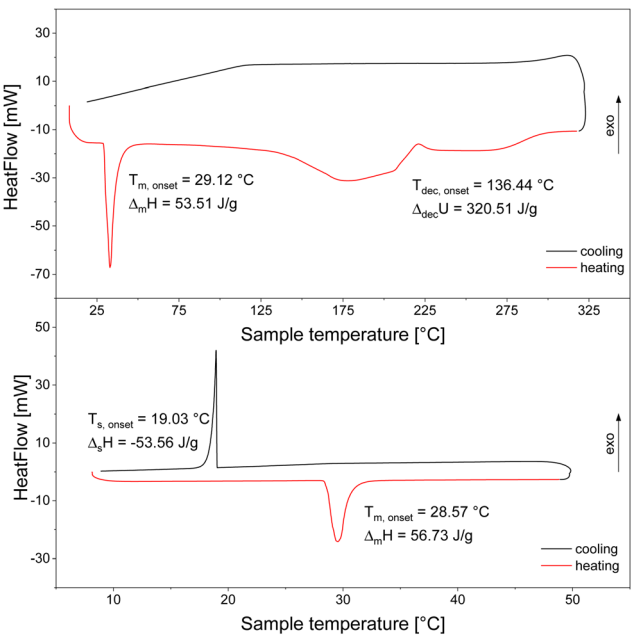

Fig. 2 DSC measurements to investigate the melting (bottom; heating/cooling rate of 1 K min^{-1} from 8 °C to 50 °C; 33.50 mg sample) and decomposition behaviour (top; heating/cooling rate of 5 K min^{-1} from 8 °C to 325 °C; 58.87 mg sample) of $Hf(BH_4)_4$ in closed crucibles.

Table 4 Summary of the measured temperatures both for melting T_m and decomposition T_{dec} of $Hf(BH_4)_4$ with literature values (CVD: chemical vapour deposition)

T_m [°C]	Method	T_{dec} [°C]	Method	Ref.
29.0	Vapor pressure	—	—	3
29	Not mentioned	—	—	56
—	—	100	CVD	5
—	—	200	CVD	8
28.43	DSC	136.44	DSC	This work

Table 4 serves as a summary of all so far reported melting and decomposition temperatures.

Investigation of the decomposition behaviour and the decomposition products using TG-DSC-MS and P-XRD

After the DSC experiment the remaining materials were removed from the crucibles under inert conditions providing a coarse black powder in both cases, the $Zr(BH_4)_4$ and the $Hf(BH_4)_4$ one. In the following X-ray powder diffraction measurements we did not observe any sharp reflections that could have been clearly assigned to a reference pattern (see Fig. 3).

SEM-EDX investigations were carried out after combining the sets of all Zr and of all Hf containing samples each to one sample. The joint Zr sample displays a much coarser morphology than the Hf one showing almost spherical particles giving the appearance that the material has undergone a melting process supporting the conclusion from the DSC measurement that the decomposition occurred from the melt. Although the DSC measurement indicates a decomposition from the melt as well, the morphology of the material in the joint Hf sample does not support this interpretation in the same way the joint Zr sample does. The particles or agglomerates in the joint Hf sample are much smaller and are not of spherical or particularly roundish appearance (see ESI† Fig. S5). However, this result does not necessarily contradict the occurrence of the melting process because in contrast to a pure melting and recrystallisation process the material also underwent a decomposition reaction. There is a composition of about (85 ± 3) atom–% boron and (15 ± 3) atom–% Zr and (81 ± 3) atom–% boron and (19 ± 3) atom–% Hf, respectively. By assuming that the EDX analysis measures also a significant portion of the bulk phase (see Fig. S5, ESI†) and taking into account the error of the EDX investigation, the expected ratio of metal to boron of 1:4 can be seen as supported. The postulated decomposition processes of $Zr(BH_4)_4$ in the CVD process described by Sung *et al.*[6] and during the DSC measurement in open crucibles described by Gennari *et al.*[10] into ZrB_2, B_2H_6 and H_2 probably did not occur in our DSC measurement, because otherwise a metal to boron ratio of 1:2 would have been expected. Given that the pressure built up is the main difference between our DSC measurements and those using open crucibles or the CVD process, which were conducted at atmospheric pressure, we attributed this fact as the main factor for the observed differences. A significant difference between our experimentes and those of Gennari *et al.*[10] is the generation of hydrogen as the sole gaseous product. Therefore, no boron gets lost by diborane emmission during the decomposition and is still available for a later rehydrogenation.

In order to investigate the decomposition product mixtures generated during the DSC measurements further, we performed TG-DSC-MS measurements in the temperature range between RT and 650 °C (see Fig. 4). The heat flow signal does not exhibit large values, which is typical for amorphous compounds. The increase in the TG signals towards the end of the experiments results from the oxidation of the compounds by traces of oxygen in the argon purge gas.

There is a mass loss accompanied by the desorption of hydrogen for both samples of approximately 1.4% and 0.9% for the Zr and Hf containing sample, respectively, but no release of diborane was observed. Furthermore, the powder X-ray diffractograms of the samples after the TG-DSC-MS experiments reveal the reflections of the respective metal diborides (see Fig. 5).

The consideration of the entirety of experimental results leads to the conclusion that the decomposition of the two boranates occurs in the same manner. Firstly, they decompose

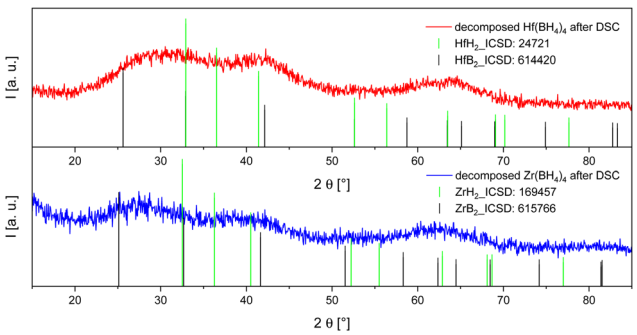

Fig. 3 P-XRD results of the decomposed samples of the DSC measurements (Zr: bottom, blue; Hf: top, red). The given reflections (metal borides: black; metal hydrides: green) were taken from the ICSD.[63]

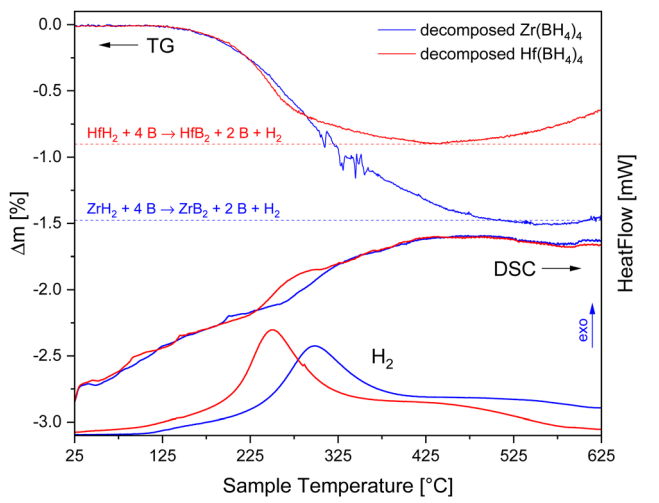

Fig. 4 TG-DSC measurements in 1 bar argon atmosphere with 5 K min^{-1} and about 10 mg sample of the decomposition products after the DSC measurements of $Zr(BH_4)_4$ and $Hf(BH_4)_4$. The hydrogen evolution was measured with MS (in a.u.).

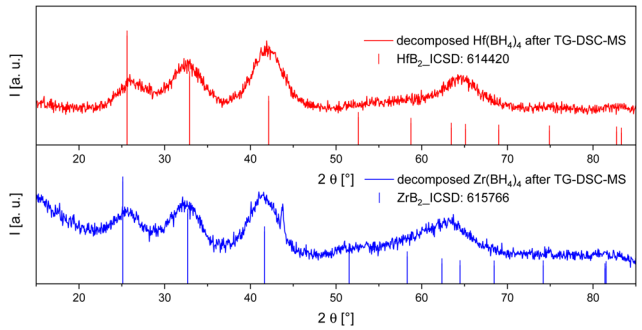

Fig. 5 Powder X-ray diffraction patterns of the decomposed MH_2-B mixtures after the hydrogen desorption in the TG-DSC-MS measurements up to 650 °C. The reference patterns were taken from the ICSD.[63]

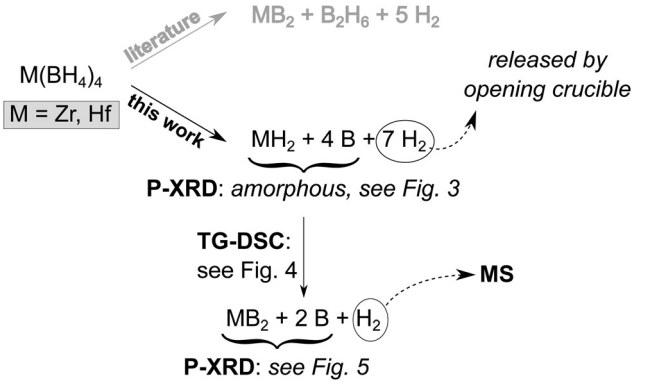

Fig. 6 Proposed decomposition reactions of $Zr(BH_4)_4$ and $Hf(BH_4)_4$ using the mentioned techniques. The literature decomposition route reported by ref. 6 and 10 was not observed during our measurements.

into hydrogen, the respective metal dihydrides and four equivalents of boron as reflected by reactions (8) and (9). Despite the decomposition into these assumed products no reflections of boron and the metal dihydrides are visible in the corresponding X-ray diffractograms, a phenomenon which is known from other boranates and their respective decomposition products, too.[1] Furthermore, it is reported by Paskevicius *et al.*[64] that boron can form stable amorphous B_{12}-clusters that would not be detectable by X-ray diffraction. Secondly, the metal dihydrides react with two equivalents of boron during the TG-DSC-MS measurements releasing hydrogen (see Fig. 4) to produce the metal diborides. Reflections of the diborides have then been seen in the corresponding powder X-ray diffraction patterns (see Fig. 5). The amounts of hydrogen released fit well to the predicted theoretical values of about 1.5% and 0.9% resulting from the reactions (10) and (11), respectively. The remaining boron was not detected by P-XRD presumably because of the reasons given above.

$$Zr(BH_4)_4 \rightarrow ZrH_2 + 4\ B + 7\ H_2 \quad (8)$$

$$Hf(BH_4)_4 \rightarrow HfH_2 + 4\ B + 7\ H_2 \quad (9)$$

$$ZrH_2 + 4\ B \rightarrow ZrB_2 + 2\ B + H_2 \quad (10)$$

$$HfH_2 + 4\ B \rightarrow HfB_2 + 2\ B + H_2 \quad (11)$$

Finally, we state the complete reaction scheme occuring during the temperature ramping in the DSC experiments. In the heating phase up to 325 °C, the decomposition occurs in accordance with reaction (8) in the case of Zr and reaction (9) in the one of Hf generating amorphous dihydrides and four equivalents of amorphous boron as solid decomposition products. Further heating up to 650 °C leads to a decomposition according to the reactions (10) and (11). One might argue that the compounds could also decompose into ZrB_2, B_2H_6 and H_2, because no reflections of boron in the powder X-ray diffractograms are observable. The SEM-EDX measurements performed after the TG-DSC-MS investigations, however, show that the obtained material is as rich of boron as at the start of the experiment (for both samples about 80 atom–% B and about 20 atom–% of the corresponding metal component; see Fig. S6 in the ESI† for the SEM images). This finding supports the view that the decomposition takes place to solid boron according to the reactions (8) and (9), because the formation of a gaseous species, like diborane, would result in the loss of this component.

Fig. 6 gives a summary of observed and proposed decomposition processes.

Assuming the reactions (8) and (9), it is possible to determine the decomposition enthalpy $\Delta_{dec}H$. For this purpose eqn (12) was employed using the measured reaction heats accompanying these processes (see Fig. 1 and 2).

$$\Delta_{dec}H = \Delta_{dec}U + R \cdot T_{dec,onset} \cdot \sum_i \nu_{i,gas} \quad (12)$$

For $Zr(BH_4)_4$ and $Hf(BH_4)_4$ one obtains $\Delta_{dec}H(403.42\ K) = 80.4\ kJ\ mol^{-1}$ and $\Delta_{dec}H(409.58\ K) = 100.1\ kJ\ mol^{-1}$, respectively.

Heat capacity measurements

The heat capacity measurements of the two boranates were conducted in the temperature range from approximately 280 K

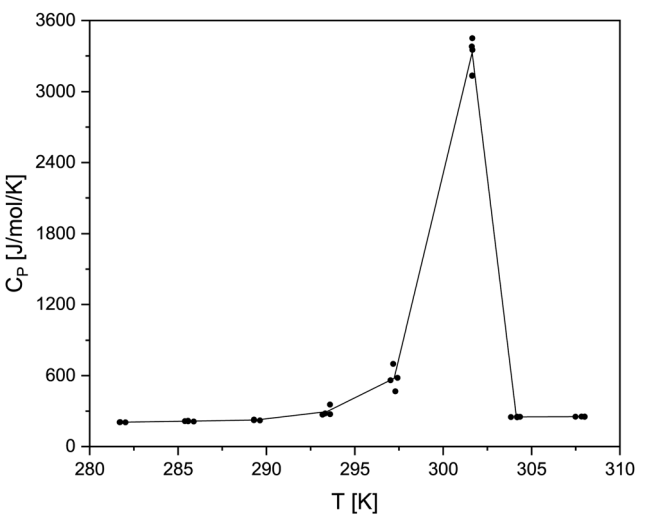

Fig. 7 Graph of the measured C_P values for $Zr(BH_4)_4$ in the temperature range from 280 to 310 K (black dots; black line is drawn to guide the readers eyes).

to 310 K allowing to determine values regarding the solid and the liquid phase. At temperatures higher than about 310 K there have been leakage problems with the crucibles used. The compounds exhibit significant pre-melting effects, which can be seen exemplarily for $Zr(BH_4)_4$ in Fig. 7.

The occurrence of such a pre-melting effect, *i.e.* the increase of the heat capacity prior to the actual melting, is a phenomenon also known for other systems.[65] In regard to the determination of the heat capacities of the liquid and the solid phase close to the phase transition, this pre-melting effect has the consequence that only rather few data points can be seen as unaffected by the phase transition. Because of this behaviour only three data points for $Zr(BH_4)_4$ and four for $Hf(BH_4)_4$ are available for the solid phase. For the liquid phase only two data points are available for $Zr(BH_4)_4$ and only one for $Hf(BH_4)_4$. The obtained heat capacity values for both compounds in the temperature range between app. 280 to 310 K are listed in the ESI† in Table S1. For the fit of the C_P values of the solid and the liquid phase, we used a linear function as stated in eqn (13).

$$C_P = A + B{\cdot}T \quad (13)$$

The fitting coefficients and fit quality parameters *FitStdErr* (fit standard error) of the heat capacity functions for both compounds are summarised in Table 5. Each DSC measurement was repeated four times.

To obtain the thermodynamic values of the melting process, we extrapolated the solid and liquid heat capacity functions until the melting point. By integration of the area below the C_P/T curve over the measured temperature range we calculated (41.67 ± 0.67) J mol^{-1} K^{-1} and (32.84 ± 1.05) J mol^{-1} K^{-1} as values of the melting entropies for $Zr(BH_4)$ and $Hf(BH_4)_4$, respectively. Multiplication of those values with the melting temperature leads to the melting enthalpy of (12.57 ± 0.20) kJ mol^{-1} for $Zr(BH_4)_4$, which is in good agreement with the before mentioned value of 13.25 kJ mol^{-1} from our DSC measurements. We strongly assume that the given value from Hoekstra and Katz[3] of about 18 kJ mol^{-1} is rather erroneous because of the determination *via* vapour pressure measurements at low pressures. For $Hf(BH_4)_4$ we obtained (9.92 ± 0.30) kJ mol^{-1} for the melting enthalpy, which is lower than the value from the DSC measurement (13.49 kJ mol^{-1}). The latter fits better to the literature one of 14.24 kJ mol^{-1} provided by Hoekstra and Katz.[3] Probably, the $\Delta_F S$ value derived from the C_P measurements is smaller because of the fact that only one C_P value from the liquid phase was useable causing a large uncertainty in the integration of the C_P/T curve (see our C_P measurement of $Hf(BH_4)_4$ in Fig. S7, ESI†).

Table 5 Coefficients of molar heat capacity functions of $Zr(BH_4)_4$ and $Hf(BH_4)_4$ from 280 K to 310 K including the fit standard error

Compound	T range [K]	A [J mol^{-1} K^{-1}]	B [J mol^{-1} K^{-2}]	*FitStdErr*
$Zr(BH_4)_4$	280 to 301	$-4.20\cdot 10^2$	$2.23\cdot 0^0$	$2.34{\cdot}10^0$
	301 to 310	$9.13\cdot 10^1$	$5.24{\cdot}10^{-1}$	$144{\cdot}10^0$
$Hf(BH_4)_4$	280 to 301	$-4.72\cdot 10^1$	$9.14\cdot 10^{-1}$	$2.14\cdot 10^0$
	301 to 310	$2.59\cdot 10^2$	—	$9.03\cdot 10^{-1}$

Enthalpy of formation

Given that the decomposition of the investigated boranates proceeds according to reactions (8) and (9), the calculation of the enthalpy of formation $\Delta_F H$(298.15 K) becomes possible. The thermodynamic data needed for the calculations were taken from the HSC 5.1 database (H_2, B, ZrB_2)[66] and FactSage 7.1 (HfB_2).[67] For the determination of $\Delta_F H$(298.15 K) nearly all parameters and quantities measured so far for both compounds (T_m, $\Delta_m H$, C_P, T_{dec}, $\Delta_{dec} H$) are needed. Applying Kirchhoff's law to the reactions (8) and (9) one obtains for the enthalpies of formation $\Delta_F H$(298.15 K) = −260.6 kJ mol^{-1} for $Zr(BH_4)_4$ and $\Delta_F H$(298.15 K) = −228.0 kJ mol^{-1} for $Hf(BH_4)_4$. Nakamori *et al.*[32,33] developed a way to estimate the enthalpy of formation of boranates by exploiting the correlation between the Pauling electronegativity and this quantity. Utilising his correlation function, the value of $\Delta_F H$(298.15 K) = −240.1 kJ mol^{-1} for $Zr(BH_4)_4$ and $\Delta_F H$(298.15 K) = −270.0 kJ mol^{-1} for $Hf(BH_4)_4$ can be predicted. The values obtained by the same estimation method by Miwa *et al.*[68] and Sato *et al.*[69] are similar, whereas the values from Callini *et al.*[70] deviate with −368.8 kJ mol^{-1} for $Zr(BH_4)_4$ and −398.3 kJ mol^{-1} for $Hf(BH_4)_4$ very strongly from our data and those derived from the work of the other authors. It is important to note that the $\Delta_F H$(298.15 K) values for the reference boranates to establish such correlation functions used by Nakamori and the other authors were determined by DFT. In conclusion, there are quite large differences for both compounds between the experimental values and the predicted ones. The large variation of the predictions stresses the need for independently obtained experimental results.

Standard entropy *via* DFT

Regrettably, the entropy of decomposition could not be calculated using the measured decomposition enthalpy at the corresponding decomposition temperature because a scanning measurement is not a suitable method to determine equilibrium values. To compensate for that, DFT was used to obtain the standard entropies of both compounds based on their calculated phonon densities of states using the Quantum ESPRESSO code.[49–51]

For the two systems in question, $Zr(BH_4)_4$ and $Hf(BH_4)_4$, initial crystal structures were obtained *via* the previously described *in situ* single crystal XRD measurements. On these initial structures, convergence tests with respect to the kinetic energy cutoff of the wave function, the kinetic energy cutoff of the density and the integration grid in reciprocal space were conducted and the values for these three parameters were chosen so that any further increase would lead to a total energy difference of less than 1 meV atom^{-1}. Afterwards, the initial structures were relaxed in terms of both the nuclear positions and the cell parameters until the nuclear forces were below 0.1 mRy Bohr^{-1} and the pressure on the cell was below 0.1 kbar. Then, the optimised unit cells were volume scaled in the range of 95% to 110% of the optimised volume. For each member in this series of volumes, the nuclear positions were relaxed again according to the force convergence tolerance given detailed

above, keeping the volume fixed. As a next step, the total energy and the phonon density of states were evaluated for the series of volumes. In this procedure, the vibrational frequencies were determined for a 3 × 3 × 3 grid in reciprocal space; the results for this grid were later Fourier interpolated to a 20 × 20 × 20 grid. For each point in the 3 × 3 × 3 grid, the vibrational frequencies were calculated according to density functional perturbation theory.[71–73] With all phonon calculations finished and the phonon density of states available for each of the volumes, the Gibbs energy of $Zr(BH_4)_4$ and $Hf(BH_4)_4$ and its first temperature derivative were evaluated for a pressure of 1 bar and a temperature of 298.15 K according to the quasi-harmonic approximation. The standard entropy was calculated as the negative of the first temperature derivative, yielding $S^\circ(Zr(BH_4)_4)$ = 228.4 J mol^{-1} K^{-1} and $S^\circ(Hf(BH_4)_4)$ = 212.7 J mol^{-1} K^{-1}.

To give more reliability to our DFT calculations, the standard entropy for $LiBH_4$ at 298.15 K in its room temperature polymorph (orthorhombic according to ICSD number 239763[74]) was calculated under the same conditions, as mentioned for $Zr(BH_4)_4$ and $Hf(BH_4)_4$. The calculation gives a value of S_{DFT}(298.15 K) = 71.5 J mol^{-1} K^{-1}, which is in good agreement with the experimental value of S_{exp}(298.15 K) = 75.8 J mol^{-1} K^{-1}.[66]

Optimisation of the values based on the CalPhaD method

All of our obtained data (reaction enthalpies, specific heats, calculated entropies, enthalpies of fusion) and vapour pressure values[3] formed the basis for the optimisation *via* CalPhaD. The optimisation was carried out with the ChemSage 4.3[75] and FactSage 7.1[67] software. The optimised thermodynamic data are presented in Table 6.

Furthermore, the values of the entropy of vaporisation at the boiling points (89.7 J mol^{-1} K for $Zr(BH_4)_4$ and 92.3 J mol^{-1} K^{-1} for $Hf(BH_4)_4$) correspond very well to what would be expected applying Trouton-Pictet's rule ($\Delta_v S(T_v) \approx$ 88 J mol^{-1} K^{-1} to 90 J mol^{-1} K^{-1}).[76] It can therefore be assumed that the liquid boranates do not form associates.

With these data the vapour pressures of both compounds were calculated using DD in the manner as given in eqn (15).

$$\Delta_T G^\circ = -R \cdot T \cdot \ln\left(\frac{p_{\nu,eq}}{p^\circ}\right) \quad (14)$$

Table 6 Optimised values based on the CalPhaD method

	$Zr(BH_4)_4$	$Hf(BH_4)_4$
$\Delta_F H_s^\circ$(298.15 K) [kJ mol^{-1}]	−260.6	−228.0
$\Delta_F H_l^\circ$(298.15 K) [kJ mol^{-1}]	−248.0	−218.1
$\Delta_F H_g^\circ$(298.15 K) [kJ mol^{-1}]	−211.6	−177.8
S_s°(298.15 K) [J mol^{-1} K^{-1}]	228.4	212.7
S_l°(298.15 K) [J mol^{-1} K^{-1}]	270.1	245.4
S_g°(298.15 K) [J mol^{-1} K^{-1}]	374.8	348.7
T_m [°C]	28.8	28.9
$\Delta_m H(T_m)$ [kJ mol^{-1}]	12.6	10.0
$\Delta_m S(Z_m)$ [J mol^{-1} K^{-1}]	41.7	33.3
T_v [°C]	124.4	123.2
$\Delta_v H(T_v)$ [kJ mol^{-1}]	35.7	36.6
$\Delta_v S(T_v)$ [J mol^{-1} K^{-1}]	89.7	92.3
T_{dec} [°C]	130.4	136.4
$\Delta_{dec} H^\circ(T_{dec})$ [kJ mol^{-1}]	80.4	99.5

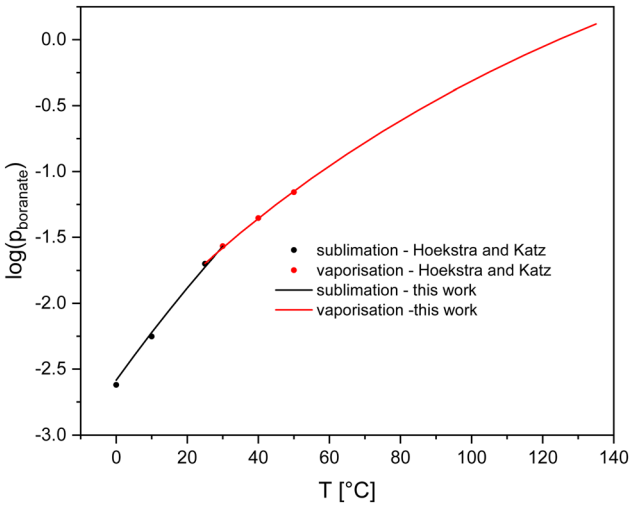

Fig. 8 Comparison between the measured vapour pressure values of Hoekstra and Katz[3] (dots) and our calculated ones (lines) for $Zr(BH_4)_4$ (sublimation: black; vaporisation: red).

$$p_{\nu,eq} = p^\circ \cdot e^{-\frac{\Delta_T G^\circ}{R \cdot T}} \quad (15)$$

$\Delta_T G^\circ$: free Gibbs energy of phase transition
$p_{\nu,eq}$: vapour pressure (vaporisation or sublimation)
p°: standard pressure, 1 bar

For comparison reasons, the vapour pressure data published by Hoekstra and Katz[3] and those calculated based on our optimised thermodynamic values are both displayed in Fig. 8 for $Zr(BH_4)_4$ and in Fig. S8 in the ESI† for $Hf(BH_4)_4$.

The calculated vapour pressure values using our optimised data are in good agreement with the experimental ones from Hoekstra and Katz[3] and therefore the optimisation was successful.

Conclusions

We synthesised $Zr(BH_4)_4$ and $Hf(BH_4)_4$ *via* solid state metathesis and determined their crystal structures slightly below their melting temperatures. With the low temperature structure data it was possible to calculate the cubic expansion coefficient which is in the order of magnitude of polymers. This fact underlines the soft character of these boranates as molecular crystals. Furthermore, their melting and decomposition behaviour from the liquid phase and the related enthalpy values were ascertained applying (TG-) DSC measurements. In combination with the measured heat capacity values of both the solid and liquid phases we determined the enthalpies of formation ($\Delta_F H^\circ$(298.15 K) = −260.59 kJ mol^{-1} for $Zr(BH_4)_4$ and $\Delta_F H^\circ$(298.15 K) = −227.99 J mol^{-1} K^{-1} for $Hf(BH_4)_4$). In regard to establish absolute entropy values, however, using a PPMS instrument it was not possible to perform low temperature calorimetry measurements because of the high volatility of the compounds and the high vaccum needed in such experiments.

Therefore, no experimental determination of the standard entropy was possible and was therefore replaced by DFT calculations (S°(298.15 K) = 228.4 J mol^{-1} for $Zr(BH_4)_4$ and S°(298.15 K) = 212.7 J mol^{-1} K^{-1} for $Hf(BH_4)_4$). Furthermore, we shed some light on the decomposition mechanism by correlating results from P-XRD, TG-DSC-MS and SEM-EDX investigations. Our results show the formation of MH_2 (M = Zr, Hf) as a first step contrary to other studies in the literature suggesting the decomposition into the diborides. This difference must be due to kinetic barriers for the formation of borides at these low temperatures.

Although both boranates cannot be used as hydrogen storage materials because of their high vapour pressure and the high stability of the decomposition products (which is supported by calculations regarding their decomposition behaviour presented in the electronic supplementary information), there is still the possibility of using them as catalyst precursors for reversible hydrogen storage in other complex hydride systems. The availability of additional thermodynamic data will help to estimate those (enthalpy of formation, entropies) of new boranates by the use of correlation functions.

Author contributions

K. Burkmann – investigation, validation, visualisation, writing – original draft. F. Habermann – validation, visualisation, writing – review & editing. E. Schumann – investigation, visualisation, writing – original draft. J. Kraus – formal analysis, writing – original draft. B. Störr – investigation, writing – review & editing. H. Schmidt – investigation, visualisation, resources, writing – original draft. E. Brendler – investigation, resources, writing – review & editing. J. Seidel – validation, writing – review & editing. K. Bohmhammel – formal analysis, validation, writing – review & editing. J. Kortus – resources, writing – review & editing. F. Mertens – conceptualisation, funding acquisition, resources, supervision, writing – review & editing

Conflicts of interest

There are no conflicts to declare.

Acknowledgements

The reported research activities have been financially supported by the Free State of Saxony (K. Burkmann, Landesstipendium zur Graduiertenförderung). We also thank the Deutsche Forschungsgemeinschaft (DFG) for financial support (Project ID 449160425). The authors would like to thank Dr. Lesia Sandig-Predzymirska for translating several Russian-language papers. Furthermore, the authors would like to thank Dr. M. Gerwig for the help with the preparation of the samples for the single crystal XRD measurements, Dr. J. Wagler for the help with the preparation of NMR samples, Dr. I. Paschke for several powder XRD measurements, Prof. Dr. R. Gumeniuk and Dr. M. Schwarz for numerous discussions for manufacturing of sample crucibles and A. Obst for the SEM-EDX measurements. Additionally, the authors would like to thank the URZ in Freiberg for computational time and support. The computations at the URZ were performed on the compute cluster of the Faculty of Mathematics and Computer Science of the Technische Universität Bergakademie Freiberg; this cluster is funded by the DFG - Project ID 397252409.

Notes and references

1 K. Suárez-Alcántara and J. R. Tena García, *Materials*, 2021, **14**, 2561–2616.
2 F. Habermann, K. Burkmann, B. Hansel, B. Störr, C. Schimpf, J. Seidel, M. Bertau and F. Mertens, *Dalton Trans.*, 2023, **52**, 4880–4890.
3 H. R. Hoekstra and J. J. Katz, *J. Am. Chem. Soc.*, 1949, **71**, 2488–2492.
4 G. W. Rice and R. L. Woodin, *J. Am. Chem. Soc.*, 1988, **71**, 181–183.
5 A. L. Wayda, L. F. Schneemeyer and R. L. Opila, *Appl. Phys. Lett.*, 1988, **53**, 361–363.
6 J. Sung, D. M. Goedde, G. S. Girolami and J. R. Abelson, *J. Appl. Phys.*, 2002, **91**, 3904–3911.
7 Y. Yang, S. Jayaraman, D. Y. Kim, G. S. Girolami and J. R. Abelson, *Chem. Mater.*, 2006, **18**, 5088–5096.
8 S. Jayaraman, Y. Yang, D. Y. Kim, G. S. Girolami and J. R. Abelson, *J. Vac. Sci. Technol., A*, 2005, **23**, 1619–1625.
9 S. Jayaraman, J. E. Gerbi, Y. Yang, D. Y. Kim, A. Chatterjee, P. Bellon, G. S. Girolami, J. P. Chevalier and J. R. Abelson, *Surf. Coat. Technol.*, 2006, **200**, 6629–6633.
10 F. C. Gennari, L. Fernández Albanesi and I. J. Rios, *Inorg. Chim. Acta*, 2009, **362**, 3731–3737.
11 G. A. Nesterov, V. A. Zakharov, V. V. Volkov and K. G. Myakishev, *J. Mol. Catal.*, 1986, **36**, 253–269.
12 J. J. Vajo, F. Mertens, C. C. Ahn, R. C. Bowman and B. Fultz, *J. Phys. Chem. B*, 2004, **108**, 13977–13983.
13 J. J. Vajo, S. L. Skeith and F. Mertens, *J. Phys. Chem. B*, 2005, **109**, 3719–3722.
14 M. Dornheim, S. Doppiu, G. Barkhordarian, U. Boesenberg, T. Klassen, O. Gutfleisch and R. Bormann, *Scr. Mater.*, 2007, **56**, 841–846.
15 U. Bösenberg, S. Doppiu, L. Mosegaard, G. Barkhordarian, N. Eigen, A. Borgschulte, T. R. Jensen, Y. Cerenius, O. Gutfleisch, T. Klassen, M. Dornheim and R. Bormann, *Acta Mater.*, 2007, **55**, 3951–3958.
16 Y. Suttisawat, P. Rangsunvigit, B. Kitiyanan, N. Muangsin and S. Kulprathipanja, *Int. J. Hydrogen Energy*, 2007, **32**, 1277–1285.
17 B. D. James and B. E. Smith, *Synth. React. Inorg. Met.-Org. Chem.*, 1974, **4**, 461–465.
18 B. G. Sayer, J. I. A. Thompson, N. Hao, T. Birchall, D. R. Eaton and M. J. McGlinchey, *Inorg. Chem.*, 1981, **20**, 3748–3750.
19 B. E. Smith, H. F. Shurvell and B. D. James, *Phys. Rev. B: Condens. Matter Mater. Phys.*, 1978, **710**.
20 R. W. Broach, I. S. Chuang, T. J. Marks and J. M. Williams, *Inorg. Chem.*, 1983, **22**, 1081–1084.

21 W. E. Reid, J. M. Bish and A. Brenner, *J. Electrochem. Soc.*, 1957, **104**, 21–29.
22 R. H. Banks and N. Edelstein, *J. Chem. Phys.*, 1980, **73**, 3589–3599.
23 B. D. James, R. K. Nanda and M. G. H. Wallbridge, *J. Chem. Soc. A*, 1966, 182–184.
24 N. Davies, D. Saunders and M. G. H. Wallbridge, *J. Chem. Soc. A*, 1970, 2915–2917.
25 T. J. Marks and L. A. Shimp, *J. Am. Chem. Soc.*, 1972, **94**, 1542–1550.
26 E. R. Bernstein and T. A. Keiderling, *J. Chem. Phys.*, 1973, **59**, 2105–2122.
27 N. Davies, M. G. H. Wallbridge, B. E. Smith and B. D. James, *Phys. Rev. B: Solid State*, 1973, 162–165.
28 T. A. Keiderling and W. C. Schulz, *Chem. Phys. Lett.*, 1980, **71**, 123–126.
29 A. Haaland, D. J. Shorokhov, A. V. Tutukin, H. V. Volden, O. Swang, G. S. McGrady, N. Kaltsoyannis, A. J. Downs, C. Y. Tang and J. F. C. Turner, *Inorg. Chem.*, 2002, **41**, 6646–6655.
30 J. C. Green, M. de Simone, M. Coreno, A. Jones, H. M. I. Pritchard and G. S. McGrady, *Inorg. Chem.*, 2005, **44**, 7781–7793.
31 L. H. Rude, M. Corno, P. Ugliengo, M. Baricco, Y.-S. Lee, Y. W. Cho, F. Besenbacher, J. Overgaard and T. R. Jensen, *J. Phys. Chem. C*, 2012, **116**, 20239–20245.
32 Y. Nakamori, K. Miwa, A. Ninomiya, H. Li, N. Ohba, S.-I. Towata, A. Züttel and S.-I. Orimo, *Phys. Rev. B: Condens. Matter Mater. Phys.*, 2006, **74**, 045126.
33 Y. Nakamori, H.-W. Li, M. Matsuo, K. Miwa, S. Towata and S. Orimo, *J. Phys. Chem. Solids*, 2008, **69**, 2292–2296.
34 V. V. Volkov and K. G. Myakishev, *Inorg. Chim. Acta*, 1999, **289**, 51–57.
35 U. Böhme, *Inertgastechnik*, De Gruyter, Oldenbourg, 2020.
36 D. F. Shriver and M. A. Drezdzon, *The manipulation of air-sensitive compounds*, Wiley, New York, NY, 2nd edn, 1986.
37 U. Böhme and K.-H. Thiele, *Z. Anorg. Allg. Chem.*, 1994, **620**, 1455–1462.
38 M. Gerwig, U. Böhme, M. Friebel, F. Gründler, G. Franze, M. Rosenkranz, H. Schmidt and E. Kroke, *ChemistryOpen*, 2020, **9**, 762–773.
39 D. Thomas, M. Abdel-Hafiez, T. Gruber, R. Hüttl, J. Seidel, A. U. Wolter, B. Büchner, J. Kortus and F. Mertens, *J. Chem. Thermodyn.*, 2013, **64**, 205–225.
40 D. Thomas, M. Zeilinger, D. Gruner, R. Hüttl, J. Seidel, A. U. Wolter, T. F. Fässler and F. Mertens, *J. Chem. Thermodyn.*, 2015, **85**, 178–190.
41 S. Loos, D. Gruner, M. Abdel-Hafiez, J. Seidel, R. Hüttl, A. U. Wolter, K. Bohmhammel and F. Mertens, *J. Chem. Thermodyn.*, 2015, **85**, 77–85.
42 F. Taubert, S. Schwalbe, J. Seidel, R. Hüttl, T. Gruber, R. Janot, M. Bobnar, R. Gumeniuk, F. Mertens and J. Kortus, *Int. J. Mater. Res.*, 2017, **108**, 942–958.
43 F. Taubert, J. Seidel, R. Hüttl, M. Bobnar, R. Gumeniuk and F. Mertens, *J. Chem. Thermodyn.*, 2018, **116**, 323–329.
44 F. Taubert, J. Seidel, R. Hüttl, M. Bobnar, R. Gumeniuk and F. Mertens, *J. Chem. Thermodyn.*, 2019, **130**, 119–128.
45 K. Burkmann, B. Hansel, F. Habermann, B. Störr, M. Bertau and F. Mertens, *Z. Naturforsch. B*, 2023, **78**, 575–578.
46 G. Della Gatta, M. J. Richardson, S. M. Sarge and S. Stølen, *Pure Appl. Chem.*, 2006, **78**, 1455–1476.
47 P. Hohenberg and W. Kohn, *Phys. Rev.*, 1964, **136**, B864–B871.
48 W. Kohn and L. J. Sham, *Phys. Rev.*, 1965, **140**, A1133–A1138.
49 P. Giannozzi, S. Baroni, N. Bonini, M. Calandra, R. Car, C. Cavazzoni, D. Ceresoli, G. L. Chiarotti, M. Cococcioni, I. Dabo, A. D. Corso, S. de Gironcoli, S. Fabris, G. Fratesi, R. Gebauer, U. Gerstmann, C. Gougoussis, A. Kokalj, M. Lazzeri, L. Martin-Samos, N. Marzari, F. Mauri, R. Mazzarello, S. Paolini, A. Pasquarello, L. Paulatto, C. Sbraccia, S. Scandolo, G. Sclauzero, A. P. Seitsonen, A. Smogunov, P. Umari and R. M. Wentzcovitch, *J. Phys.: Condens. Matter.*, 2009, **21**, 395502.
50 P. Giannozzi, O. Andreussi, T. Brumme, O. Bunau, M. Boungiorno Nardelli, M. Calandra, R. Car, C. Cavazzoni, D. Ceresoli, M. Cococcioni, N. Colonna, I. Carnimeo, A. D. Corso, S. de Gironcoli, P. Delugas, R. A. DiStasio Jr, A. Ferretti, A. Floris, G. Fratesi, G. Fugallo, R. Gebauer, U. Gerstmann, F. Giustino, T. Gorni, J. Jia, M. Kawamura, H.-Y. Ko, A. Kokalj, E. Küçükbenli, M. Lazzeri, M. Marsili, N. Marzari, F. Mauri, N. L. Nguyen, H.-V. Nguyen, A. Otera-de-la Roza, L. Paulatto, S. Poncé, D. Rocca, R. Sabatini, B. Santra, M. Schlipf, A. P. Seitsonen, A. Smogunov, I. Timrov, T. Thonhauser, P. Umari, N. Vast, X. Wu and S. Baroni, *J. Phys.: Condens. Matter.*, 2017, **29**, 465901.
51 P. Giannozzi, O. Baseggio, P. Bonfà, D. Brunato, R. Car, I. Carnimeo, C. Cavazzoni, S. de Gironcoli, P. Delugas, F. F. Ruffino, A. Ferretti, N. Marzari, I. Timrov, A. Urru and S. Baroni, *J. Chem. Phys.*, 2020, **152**, 154105.
52 P. E. Blöchl, *Phys. Rev. B: Condens. Matter Mater. Phys.*, 1994, **50**, 17953–17979.
53 A. D. Corso, *Comput. Mater. Sci.*, 2014, **95**, 337–350.
54 J. P. Perdew, K. Burke and M. Ernzerhof, *Phys. Rev. Lett.*, 1996, **77**, 3865–3868.
55 H. Nöth and B. Wrackmeyer, *Nuclear Magnetic Resonance Spectroscopy of Boron Compounds*, Springer, Berlin and Heidelberg, 1978, vol. 14.
56 M. Ehemann and H. Nöth, *Z. Anorg. Allg. Chem.*, 1971, **386**, 87–101.
57 Z. Odziana, P. Blonski, Y. Yan, D. Rentsch and A. Remhof, *J. Phys. Chem. C*, 2014, **118**, 6594–6603.
58 T. Parella, *eNMR: NMR Periodic Table*, 2003, **https://triton.iqfr.csic.es/guide/eNMR/chem/NMRnuclei.html**.
59 P. Coppens, in *Crystallographic computing*, ed. F. R. Ahmed, S. R. Hall and C. P. Huber, Munksgaard, Copenhagen, 1970, pp. 255–270.
60 A. M. Igoshkin, I. F. Golovnev, V. V. Krisyuk and I. K. Igumenov, *J. Struct. Chem.*, 2016, **57**, 1068–1073.
61 G. Grimvall, *Thermophysical properties of materials*, Elsevier, Amsterdam, 1st edn, 1999.
62 *CRC Handbook of chemistry and physics*, ed. W. M. Haynes, CRC Press, Boca Raton and London and New York, 97th edn, 2017.

63 G. Bergerhoff and I. D. Brown, in *Crystallographic Databases*, ed. F. H. Allen *et al.*, International Union of Crystallography, Chester, 1987.
64 M. Paskevicius, L. H. Jepsen, P. Schouwink, R. Cerný, D. B. Ravnsbæk, Y. Filinchuk, M. Dornheim, F. Besenbacher and T. R. Jensen, *Chem. Soc. Rev.*, 2017, **46**, 1565–1634.
65 J. Acker, S. Köther, K. M. Lewis and K. Bohmhammel, *Silicon Chem.*, 2003, **2**, 195–206.
66 A. Roine, *HSC Chem.*, 2002.
67 C. W. Bale, E. Bélisle, P. Chartrand, S. A. Decterov, G. Eriksson, A. E. Gheribi, K. Hack, I. H. Jung, Y. B. Kang, J. Melançon, A. D. Pelton, S. Petersen, C. Robelin, J. Sangster, P. Spencer and M. A. van Ende, *Calphad*, 2016, **54**, 35–53.
68 K. Miwa, N. Ohba, S.-I. Towata, Y. Nakamori, A. Züttel and S.-I. Orimo, *J. Alloys Compd.*, 2007, **446–447**, 310–314.
69 T. Sato, K. Miwa, Y. Nakamori, K. Ohoyama, H.-W. Li, T. Noritake, M. Aoki, S.-I. Towata and S.-I. Orimo, *Phys. Rev. B: Condens. Matter Mater. Phys.*, 2008, **77**, 1041141.
70 E. Callini, Z. Ö. K. Atakli, B. C. Hauback, S.-I. Orimo, C. Jensen, M. Dornheim, D. Grant, Y. W. Cho, P. Chen, B. Hjörvarsson, P. de Jongh, C. Weidenthaler, M. Baricco, M. Paskevicius, T. R. Jensen, M. E. Bowden, T. S. Autrey and A. Züttel, *Appl. Phys. A: Mater. Sci. Process.*, 2016, **122**, 353–375.
71 S. Baroni, P. Giannozzi and A. Testa, *Phys. Rev. Lett.*, 1987, **59**, 2662–2665.
72 S. Y. Savrasov, *Phys. Rev. B: Condens. Matter Mater. Phys.*, 1996, **54**, 16470–16486.
73 X. Gonze and C. Lee, *Phys. Rev. B: Condens. Matter Mater. Phys.*, 1997, **55**, 10355–10368.
74 E. Roedern, Y.-S. Lee, M. B. Ley, K. Park, Y. W. Cho, J. Skibsted and T. R. Jensen, *J. Mater. Chem. A*, 2016, **4**, 8793–8802.
75 G. Eriksson, K. Hack, M. Philipps and C. Fullerton-Batten, *Chemsage - Gibbs Energy Minimizer and Optimazation Routine*, database.
76 G. Wedler, *Lehrbuch der Physikalischen Chemie*, Wiley-VCH, Weinheim, 5th edn, 2004.

